Analysis, Design, and Control of an
Omnidirectional Mobile Robot in Rough Terrain

by

Martin Richard Udengaard

B.S., Mechanical Engineering (2002)
B.A., Physics (2002)

The University of Texas at Austin

Submitted to the Department of Mechanical Engineering
in Partial Fulfillment of the Requirements for the Degree of
Master of Science in Mechanical Engineering

at the

Massachusetts Institute of Technology
[June 2008]
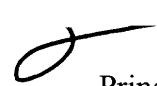© 2008 Massachusetts Institute of Technology

Signature of Author ....:..
<div align="right">Department of Mechanical Engineering</div>
<div align="right">May 9, 2008</div>
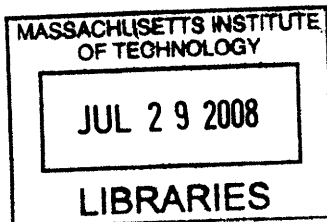
Certified by ....
<div align="right">Karl Iagnemma</div>
<div align="right">Principal Research Scientist</div>
<div align="right">Thesis Supervisor</div>

Accepted by ....,
<div align="right">Lalit Anand</div>
<div align="right">Professor of Mechanical Engineering</div>
<div align="right">Chairman, Department Committee on Graduate Students</div>

ACKNOWLEDGEMENTS

I would like to thank my advisor, Karl Iagnemma. His patience and guidance have helped me grow as a researcher, and will hopefully prepare me for success in the 'real world.'

I thank my parents, Niels and Susana, for their continuing support and for instilling in me the importance of education.

Most of all, I would like to my wife, Alice. Knowing that she will always be there no matter what life brings gives me great comfort. Watching her devotion to helping others inspires me to focus my research on helpful technologies.

Analysis, Design, and Control of an Omnidirectional Mobile Robot in Rough Terrain

by

Martin Richard Udengaard

Submitted to the Department of Mechanical Engineering
on May 9th, 2008 in Partial Fulfillment of the
Requirements for the Degree of Master of Science in
Mechanical Engineering

ABSTRACT

An omnidirectional mobile robot is able, kinematically, to move in any direction regardless of current pose. To date, nearly all designs and analyses of omnidirectional mobile robots have considered the case of motion on flat, smooth terrain. In this thesis, an investigation of the suitability of an active split offset caster driven omnidirectional mobile robot for use in rough terrain is presented. Kinematic and geometric properties of the drive mechanism are investigated along with guidelines for designing the robot. An optimization method is implemented to explore the design space. These analyses can be used as design guidelines for development of an omnidirectional mobile robot that can operate in unstructured environments. A simple kinematic controller that considers the effects of terrain unevenness via an estimate of the wheel-terrain contact angles is also presented. It is shown in simulation that under the proposed control method, near-omnidirectional tracking performance is possible even in rough, uneven terrain.

Thesis Supervisor: Karl Iagnemma
Title: Principal Research Scientist

TABLE OF CONTENTS

I. INTRODUCTION

Mobile robots are finding increasing use in military [1], disaster recovery [2], and exploration applications [3]. These applications frequently require operation in rough, unstructured terrain. Currently, most mobile robots designed for these applications are tracked or Ackermann-steered wheeled vehicles. Methods for controlling these types of robots in both smooth and rough terrain have been well studied [4-6]. While these robots types can perform well in many scenarios, navigation in cluttered, rocky, or obstacle-dense urban environments can be difficult or impossible. This is partly due to the fact that traditional tracked and wheeled robots must reorient to perform some maneuvers, such as lateral displacement. Omnidirectional mobile robots could potentially navigate faster and more reliably through cluttered urban environments and over rough terrain, due to their ability to track near-arbitrary motion profiles.

An omnidirectional mobile robot is able, kinematically, to move in any direction regardless of current pose. Previous researchers have proposed and developed omnidirectional mobile robots employing a wide variety of wheel types including roller [7, 8], Mecanum [9, 10], and spherical wheels [11, 12].

Roller wheel designs, as shown in Figure 1, employ small rollers along the outer edge of a "primary" wheel to allow traction in the wheel's longitudinal direction and free rolling in the lateral direction. Omnidirectional motion is obtained by orienting several of these wheels in different directions. These wheels are inexpensive, easy to control, and operate well in flat, indoor environments.
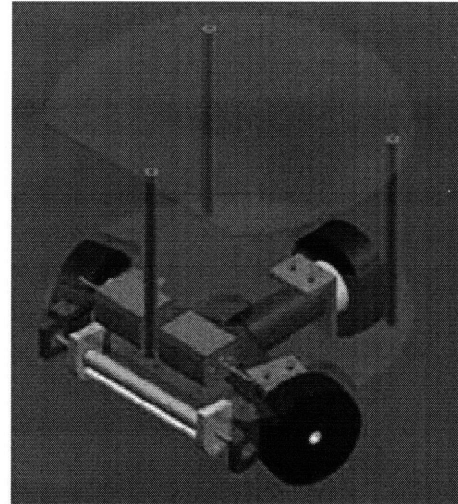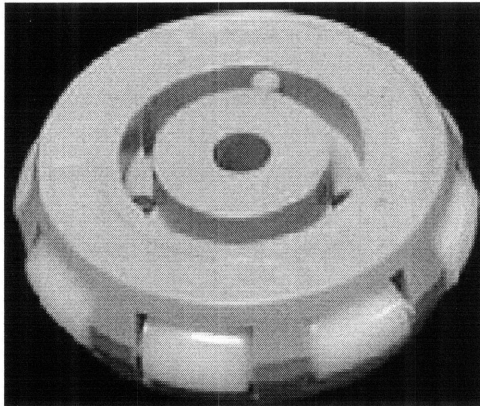
5

Figure 1. An example of a sliding wheel (left) and a possible wheel configuration to achieve omnidirectional motion (right) (from [8]).

Mecanum wheels are similar to roller wheels in that they employ rollers along the outer edge of a wheel; however the rollers are aligned at an angle to produce angular contact forces with the ground. Robots equipped with four Mecanum wheels, as shown in Figure 2, can produce omnidirectional motion (see Figure 3). Again, these wheel types have proved to be simple to control and effective on flat, clean terrain.

Roller and Mecanum wheels are unsuitable for outdoor environments, where debris can clog the rollers and alter the friction characteristics of the wheels [13]. Also, the (relatively) small rollers on the edge of each primary wheel can be subjected to significant loads, which can lead to high ground pressure and large sinkage in deformable outdoor terrain.
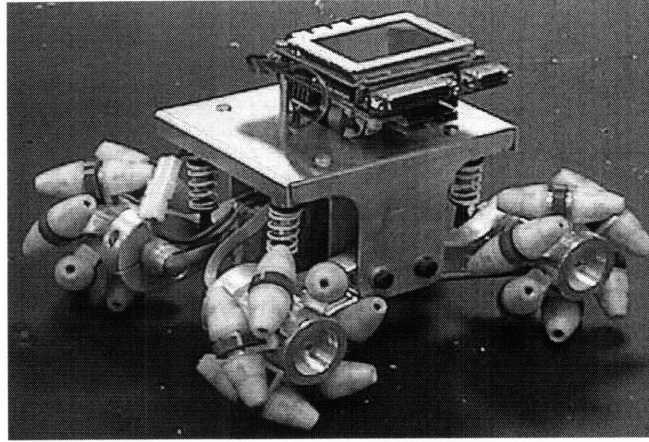
Figure 2. An example of a robot using four Mecanum wheels [9].
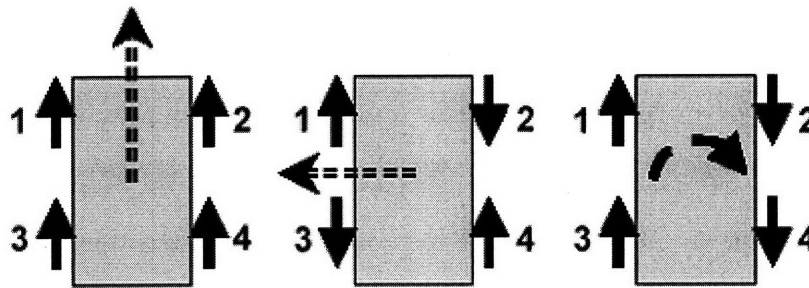
Figure 3. A schematic showing the omnidirectional capabilities of a Mecanum wheel driven omnidirectional robot (from [9]).

Spherical wheel designs, as shown in Figure 4, employ frictional drive rollers to allow rolling in any direction. Since the drive rollers rely on friction to transmit energy to the wheel, debris could potentially foul the transmission mechanism in rough, outdoor environments. Due to the two dimensional curvature of the sphere, the contact patch is smaller than that of a traditional wheel, increasing ground pressure.

Figure 4. A schematic showing a spherical wheel (left) and its use on an omnidirectional wheelchair (right) (from [12]).

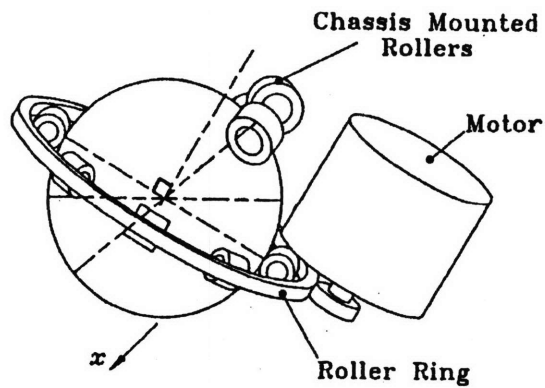Near-omnidirectional motion has been achieved using steerable wheels [14]. As shown in Figure 5, these designs have a wheel mounted to an orthogonal steering actuator. The steering actuator can rotate the wheel to point it in any planar direction. These wheels can employ standard tires, and have proven effective in outdoor environments. However they are not truly omnidirectional (i.e. the resulting robot kinematics are subject to nonholonomic constraints) since they must undergo wheel slip and/or scrubbing to change direction. This can result in deteriorated path tracking and substantial energy loss. Note that similar designs based on offset caster wheels do allow omnidirectional motion with standard tires [15]. Analysis of this design has been studied extensively for operation on flat ground.
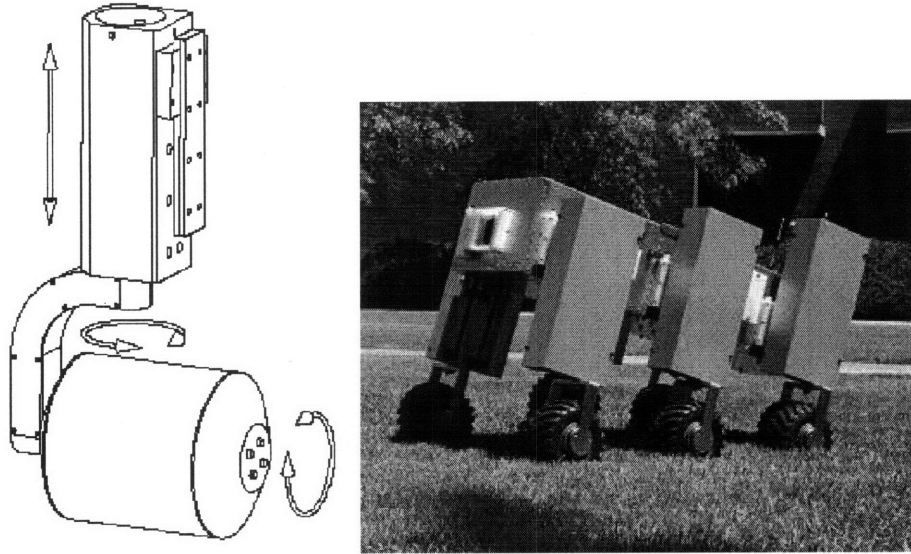
Figure 5. A schematic showing a steerable wheel (left) and its use on an outdoor mobile robot (right) (from [14]).

An omnidirectional mobile robot driven by active split offset casters (ASOCs) was initially proposed in [16] for use in structured, indoor environments. ASOC drives employ conventional wheel designs that do not rely on frictional contact, and are thus potentially suitable for use in dirty, outdoor environments. They can also be designed with little constraint on wheel diameter and width, and thus can potentially tolerate large loads with low ground pressure. Finally, ASOC modules can be integrated with suspension systems that allow for traversal of uneven terrain [17]. Therefore ASOC-driven omnidirectional mobile robots hold promise for use in rough, unstructured environments.

In this thesis, an investigation of the suitability of an ASOC-driven omnidirectional mobile robot for use in rough terrain is presented. This thesis is organized as follows: in Section II, kinematic and geometric properties of the drive mechanism are investigated, in Section III, guidelines for robot design are presented and an optimization method is implemented to explore the design space, and in Section IV, a

simple kinematic controller that considers the effects of terrain unevenness via an estimate of the wheel-terrain contact angles is presented. These analyses can be used as design guidelines for development of an omnidirectional mobile robot that can operate in unstructured environments. It is shown in simulation that under the proposed control method, near-omnidirectional tracking performance is possible even in rough, uneven terrain.

II. THE ACTIVE SPLIT OFFSET CASTER

Active split offset caster (ASOC) drive modules possess the ability to achieve omnidirectional motion via a driven wheel pair. Figure 6 shows the ASOC module considered in this study. The assembly consists of a split wheel pair, a connecting axle, and an offset link connecting the wheel pair to the mobile robot body. Each wheel is independently driven about the axis θ. The axle connecting the wheel pair can pivot about the axis β. The axle pivot can be passive or active, and allows the wheel pair to adapt to terrain unevenness, therefore increasing the likelihood of continuous terrain contact for each wheel even during travel on rough terrain. The wheel pair/axle assembly rotates about axis α. As with the axle pivot, the assembly rotation axis can also be active or passive. This axis connects the ASOC module to a robot body or a passive or active suspension element. L_{offset} is the distance between the axis α and the axis θ. L_{split} is the distance between the wheels.
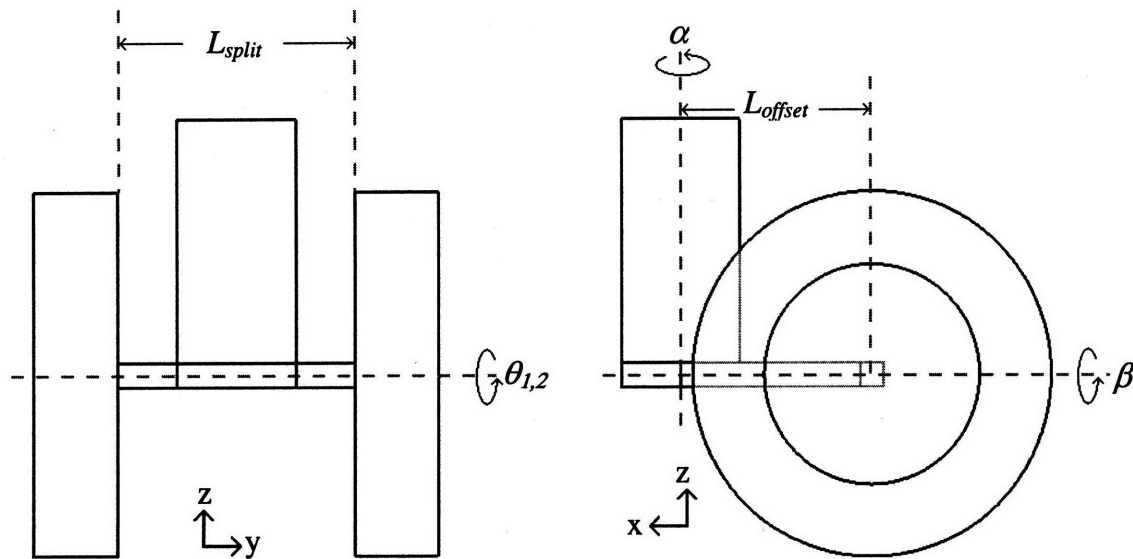

Figure 6. Active split offset caster wheel assembly front view (left) and side view (right).

By independently controlling each wheel's velocity, an ASOC module can produce arbitrary (planar) translational velocities at a point along its α axis. Two or more ASOCs attached to a rigid robot body can thus produce arbitrary translational and rotational robot velocities. Therefore, an ASOC-driven omnidirectional robot must minimally employ two ASOC modules, and can employ more to meet other design requirements related to thrust, ground pressure, tip-over stability, etc. Note that passive or active casters can also be used to augment ASOC modules to meet these requirements.

2.1 Isotropy Analysis

Path following in rough terrain may require a robot to quickly change its direction of travel. All holonomic omnidirectional mobile robots are kinematically able to instantaneously move in any planar direction. However, while some omnidirectional mobile robots exhibit preferred directions of travel, others exhibit equal mobility characteristics in all directions. Such robots are said to exhibit "isotropic mobility." Hence, isotropy is used to quantify the system's omnidirectional mobility.

Kinematic isotropy is defined as the condition in which a robot possesses a constant input velocity/output velocity ratio for all possible output velocity directions [15]. An isotropy metric is a measure of how near a robot is to the isotropy condition, and increases from 0.0 for a singular configuration (i.e. purely anisotropic, or non-omnidirectional) to 1.0 for kinematic isotropy. Ideally, an omnidirectional mobile robot should possess a metric value of 1.0 for all joint space configurations, and thus not exhibit a preferred direction of travel. This simplifies path planning and navigation by eliminating the effect of robot orientation on movement capability. The output directions

considered in this study are two planar translations in the robot body frame, and rotation about the robot body frame z axis.

The isotropy metric for a given robot configuration can be computed as the ratio of the smallest to largest eigenvalues of the Jacobian matrix relating the driving module velocities to the robot body velocities [16]. The isotropy metric can be averaged over the entire configuration space (in this case, the rotation angles between each ASOC and the body, α) to yield an average measure of performance that could be used to compare candidate omnidirectional mobile robot designs.

2.2 Effect of ASOC Geometric Parameters on Isotropy

To analyze the effect of ASOC module kinematic parameters on isotropy, variations in the wheel radius, L_{offset}, and L_{split} were analyzed over a range of values that represent a practical omnidirectional robot design space. A simple representative robot with three equally spaced modules was modeled as shown in Figure 7.
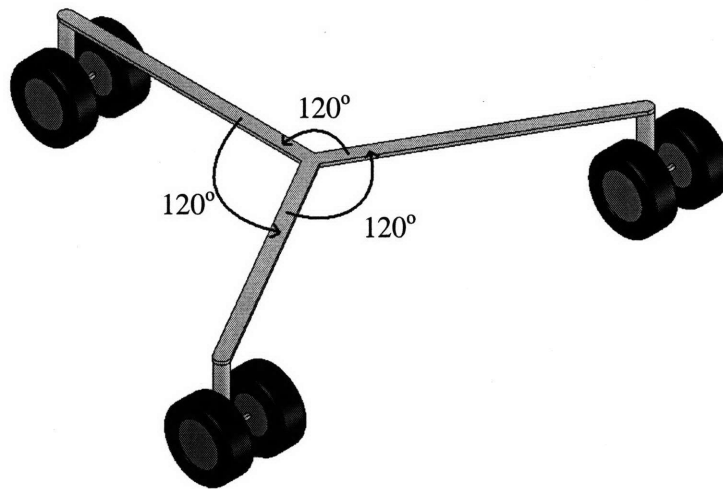

Figure 7. Simplified robot configuration for testing ASOC geometric parameters. Note that all modules are equally spaced.

The Jacobian from wheel rotational velocities to α axis translational velocities in the ASOC frame is:

$$\begin{bmatrix} v_f \\ v_s \end{bmatrix} = \begin{bmatrix} \dfrac{R_{wheel}}{2} & \dfrac{R_{wheel}}{2} \\ \dfrac{R_{wheel} \cdot L_{offset}}{L_{split}} & -\dfrac{R_{wheel} \cdot L_{offset}}{L_{split}} \end{bmatrix} \cdot \begin{bmatrix} \dot{\theta}_1 \\ \dot{\theta}_2 \end{bmatrix} \tag{1}$$

where v_f and v_s are the forward (x) and sideways (y) ASOC axis translational velocities, respectively. The wheel radius appears in each term exactly once, and therefore cancels out when the ratios of the eigenvalues are examined, thus the module isotropy is independent of the wheel radius.

In Figure 8, isotropy is shown as a function of L_{offset} and L_{split}. An iso-height exists at an isotropy value of 1.0. This iso-height occurs at L_{split} / L_{offset} =2.0. The sensitivity of isotropy to perturbations in L_{split} and L_{offset} is relatively high; a 10% change in L_{split} or L_{offset} decreases the isotropy metric value by up to 45% for small ASOC module sizes.
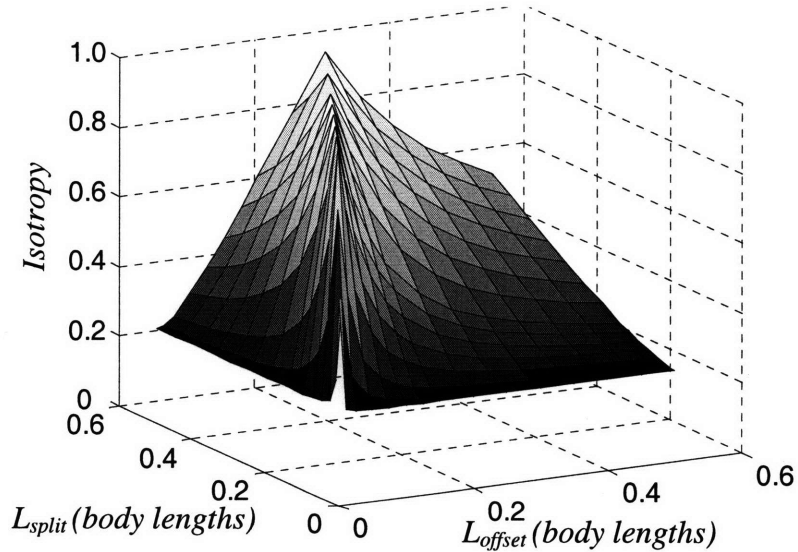

Figure 8. Average isotropy for a four ASOC omnidirectional robot.

In Figure 9, a plot of isotropy values over a range of L_{split} / L_{offset} ratios can be seen. There exists a single isotropy value for each L_{split} / L_{offset} ratio, indicating that isotropy is not an independent function of both L_{split} and L_{offset}. This is a useful insight for omnidirectional robot design. This also explains the sensitivity of isotropy to changes in L_{split} and L_{offset} for small ASOC modules sizes, since a unit change in L_{split} or L_{offset} results in a relatively large change in L_{split} / L_{offset} for small parameter values. As shown in (1), L_{split} and L_{offset} only appear as a ratio, and the Jacobian becomes isotropic when the ratio of L_{split} to L_{offset} is equal to 2.0.
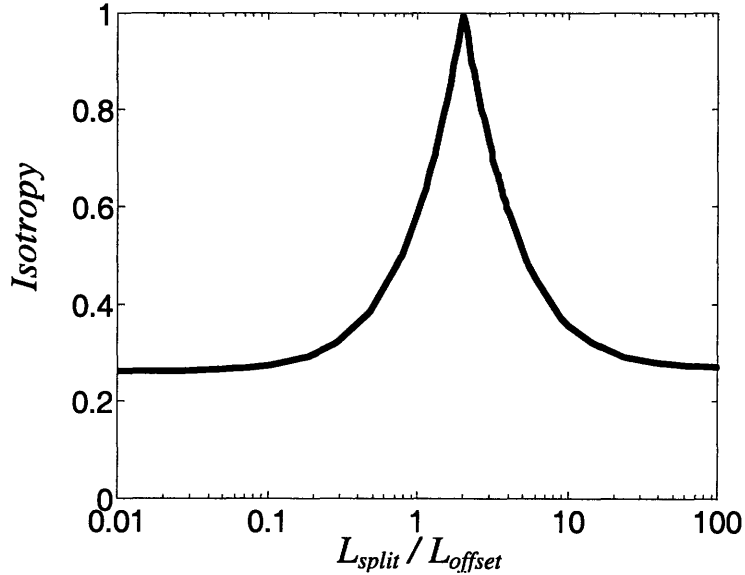
Figure 9. Average isotropy for an omnidirectional mobile robot driven by three ASOC modules as a function of L_{split} / L_{offset}.

2.3 Effect of ASOC Module Location on Isotropy

The relative location of ASOC modules with respect to one another also affects isotropy. A robot with three modules, shown in Figure 10, was chosen for analysis. A plot of isotropy as a function of relative ASOC angular location is presented in Figure 11. Each ASOC has L_{split} / L_{offset} = 2.0. ASOC physical interference was neglected.

Figure 10. Top view of representative robot for ASOC location analysis.

Figure 11. Isotropy as a function of ASOC module relative location.

16

The Jacobian of a three ASOC omnidirectional mobile robot is shown in (2). It can be seen that maximum isotropy values (1.0) are obtained when the ASOC modules are evenly spaced. The value drops to 0 for the 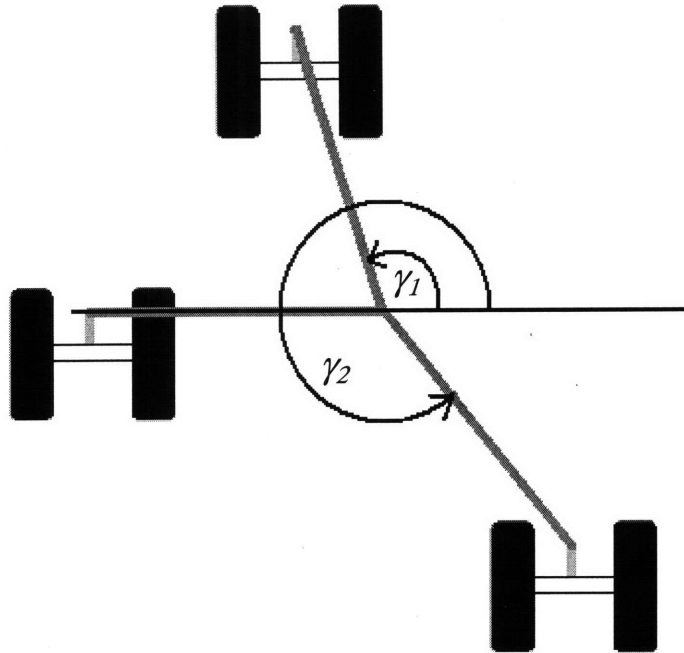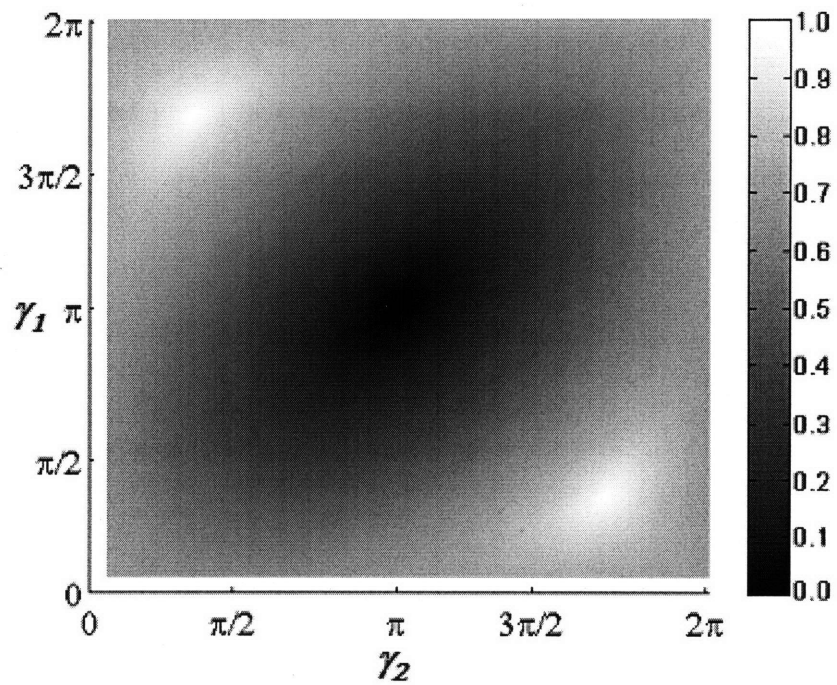degenerate case where all ASOC modules coincide. A similar phenomenon is observed for robots with any number of ASOC modules. Thus to maximize isotropy, ASOC modules should be equally spaced.

$$
J' = \frac{1}{3}
\begin{bmatrix}
\dfrac{\cos(\alpha_1)}{2} - \dfrac{L_{offset}\sin(\alpha_1)}{L_{split}} & \dfrac{\sin(\alpha_1)}{2} + \dfrac{L_{offset}\cos(\alpha_1)}{L_{split}} \\[2mm]
\dfrac{\cos(\alpha_1)}{2} + \dfrac{L_{offset}\sin(\alpha_1)}{L_{split}} & \dfrac{\sin(\alpha_1)}{2} - \dfrac{L_{offset}\cos(\alpha_1)}{L_{split}} \\[2mm]
\dfrac{\cos(\alpha_2)}{2} - \dfrac{L_{offset}\sin(\alpha_2)}{L_{split}} & \dfrac{\sin(\alpha_2)}{2} + \dfrac{L_{offset}\cos(\alpha_2)}{L_{split}} \\[2mm]
\dfrac{\cos(\alpha_2)}{2} + \dfrac{L_{offset}\sin(\alpha_2)}{L_{split}} & \dfrac{\sin(\alpha_2)}{2} - \dfrac{L_{offset}\cos(\alpha_2)}{L_{split}} \\[2mm]
\dfrac{\cos(\alpha_3)}{2} - \dfrac{L_{offset}\sin(\alpha_3)}{L_{split}} & \dfrac{\sin(\alpha_3)}{2} + \dfrac{L_{offset}\cos(\alpha_3)}{L_{split}} \\[2mm]
\dfrac{\cos(\alpha_3)}{2} + \dfrac{L_{offset}\sin(\alpha_3)}{L_{split}} & \dfrac{\sin(\alpha_3)}{2} - \dfrac{L_{offset}\cos(\alpha_3)}{L_{split}}
\end{bmatrix}
\cdots
$$

$$
\begin{bmatrix}
\dfrac{\sin(\alpha_1)}{2} + \dfrac{L_{offset}\cos(\alpha_1)}{L_{split}} \\[2mm]
\dfrac{\sin(\alpha_1)}{2} - \dfrac{L_{offset}\cos(\alpha_1)}{L_{split}} \\[2mm]
\cos(\gamma_1)\left(\dfrac{\sin(\alpha_2)}{2} + \dfrac{L_{offset}\cos(\alpha_2)}{L_{split}}\right) - \sin(\gamma_1)\left(\dfrac{\cos(\alpha_2)}{2} - \dfrac{L_{offset}\sin(\alpha_2)}{L_{split}}\right) \\[2mm]
\cos(\gamma_1)\left(\dfrac{\sin(\alpha_2)}{2} - \dfrac{L_{offset}\cos(\alpha_2)}{L_{split}}\right) - \sin(\gamma_1)\left(\dfrac{\cos(\alpha_2)}{2} + \dfrac{L_{offset}\sin(\alpha_2)}{L_{split}}\right) \\[2mm]
\cos(\gamma_2)\left(\dfrac{\sin(\alpha_3)}{2} + \dfrac{L_{offset}\cos(\alpha_3)}{L_{split}}\right) - \sin(\gamma_2)\left(\dfrac{\cos(\alpha_3)}{2} - \dfrac{L_{offset}\sin(\alpha_3)}{L_{split}}\right) \\[2mm]
\cos(\gamma_2)\left(\dfrac{\sin(\alpha_3)}{2} - \dfrac{L_{offset}\cos(\alpha_3)}{L_{split}}\right) - \sin(\gamma_2)\left(\dfrac{\cos(\alpha_3)}{2} + \dfrac{L_{offset}\sin(\alpha_3)}{L_{split}}\right)
\end{bmatrix}
\tag{2}
$$

2.4 Effect of Loss of Wheel Contact on Isotropy

When traversing rough terrain, loss of contact may occur between the wheels and the ground. In this case, system mobility will be decreased. An analysis of the isotropy of robots without full ground contact is presented in Table I. For comparison, robots with two, three, and four ASOC modules are examined. Each ASOC is allowed to possess full, partial (i.e. one wheel on the ground), or no ground contact. It is assumed that the ASOC modules are equally spaced and have $L_{split} / L_{offset} = 2.0$.

TABLE I
EFFECT OF LOSS OF WHEEL CONTACT ON ISOTROPY

Total # ASOCs	# no contact ASOCs	# partial contact ASOCs				
		0	1	2	3	4
2	0	1.000	0.464	0.000	N/A	N/A
3	0	1.000	0.706	0.504	0.270	N/A
	1	0.577	0.367	0.000	N/A	N/A
4	0	1.000	0.791	0.656	0.544	0.399
	1	0.707	0.574	0.482	0.259	N/A
	2	0.414	0.265	0.000	N/A	N/A

As expected, loss of wheel contact causes reduced isotropy due to a loss of full controllability of the ASOC modules. It can be observed that a four ASOC robot with one module that has completely lost terrain contact does not perform as well as a three ASOC robot in full contact. This is due to the fact that the three ASOC robot has equally spaced ASOC modules. Also, given an identical number of wheels without terrain contact (e.g., 0 no contact and 2 partial contact vs. 1 no contact and 0 partial contact), a robot generally has higher isotropy when terrain contact is lost on the same ASOC, since more modules remain fully engaged with the ground. The isotropy loss from partial

contact ASOC modules reinforces the importance of the axle pivot (see Figure 6).

Finally, a robot with a greater number of ASOCs will have a relatively smaller drop in isotropy for each lost wheel contact, but may have increased difficulty keeping all wheels in contact with the ground due to increased suspension complexity. Introduction of additional modules may also add mass while decreasing the allowable wheel size and available battery mass given a fixed overall system mass.

2.5 Effect of Terrain Roughness on Isotropy

Isotropy of an omnidirectional robot can also be affected by terrain roughness. Variation in terrain inclination among ASOC modules, or among ASOC module wheel pairs, causes a change in the effective value of L_{split} with respect to the body frame, which yields a change in L_{split} / L_{offset} and thus a change in isotropy (see Figure 12). Axis β allows ASOC wheels to maintain contact during travel on uneven terrain.

In theory, L_{split} could be modified as a function of terrain inclination via an active, extensible axle to cause the effective L_{split} / L_{offset} ratio to always remain near 2.0, thus yielding good isotropy characteristics on rough terrain. In practice, however, such a design would be cumbersome and impractical. Thus it is useful to examine the effects of terrain inclination on robot isotropy.
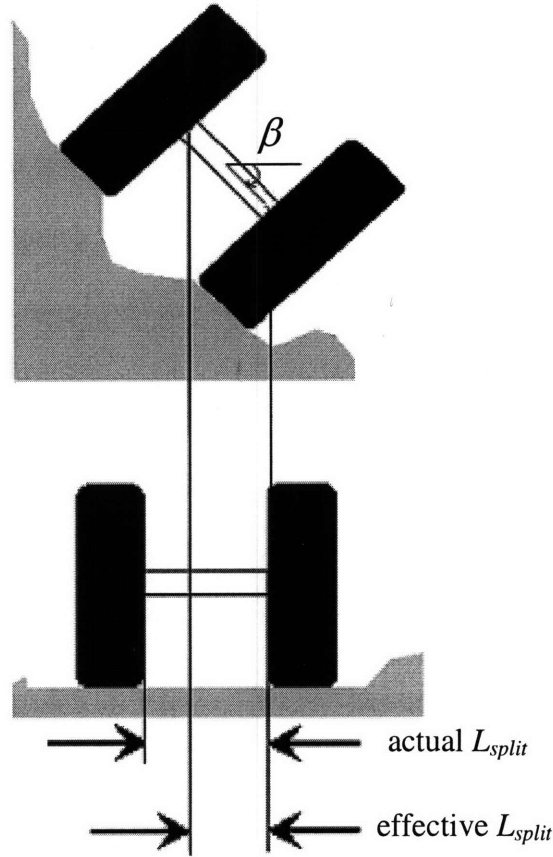
Figure 12. ASOC module on flat and rough terrain. Rough terrain can cause the module to pivot about the β axis, decreasing the effective L_{split}.

In Figure 13, a contour plot is presented of the average isotropy over a range of static robot configurations and terrain angles. The robot in this analysis had equally spaced ASOCs. The results are independent of the number of ASOC modules. The terrain angle was varied for each ASOC independently in a full factorial analysis over each terrain angle range. It can be seen that the value of L_{split} / L_{offset} with the largest isotropy value increases with the maximum terrain angle. The inclusion of pivot axle tilt in (1) produces:

$$\begin{bmatrix} v_f \\ v_s \end{bmatrix} = \begin{bmatrix} \dfrac{R_{wheel}}{2} & \dfrac{R_{wheel}}{2} \\ \dfrac{R_{wheel} \cdot L_{offset}}{L_{split} \cos(\beta)} & -\dfrac{R_{wheel} \cdot L_{offset}}{L_{split} \cos(\beta)} \end{bmatrix} \cdot \begin{bmatrix} \dot{\theta}_1 \\ \dot{\theta}_2 \end{bmatrix} \tag{3}$$

20

and it can be shown that maximum isotropy is found when:

$$\frac{L_{split}}{L_{offset}} = \frac{2}{\cos(\beta)} \qquad (4)$$

Larger angles decrease the effective ratio and thus the "true" ratio must therefore increase. Maximum average isotropy also decreases slightly with increasing terrain angle. Table II summarizes these findings.
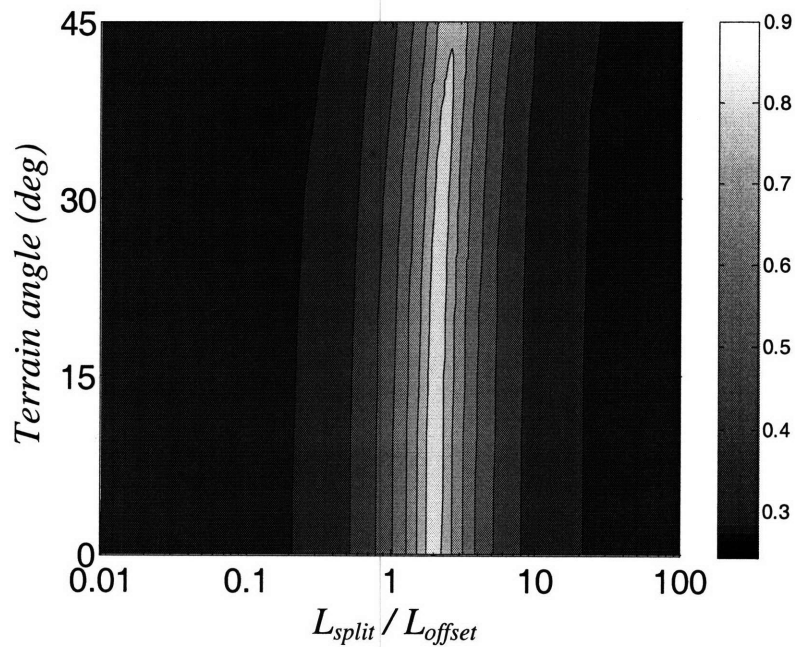

Figure 13. Average isotropy as a function of L_{split} / L_{offset} and terrain angle.

TABLE II
EFFECT OF TERRAIN ON ISOTROPY AND IDEAL SPLIT/OFFSET RATIO

Terrain angle	Max isotropy	Optimum L_{split} / L_{offset} ratio
0° (flat)	1.000	2.00
0-15°	0.987	2.05
0-30°	0.950	2.27
0-45°	0.895	2.70

III. Design of an Omnidirectional Robot for Rough Terrain

The class of robots analyzed in this thesis is man-portable, battery powered mobile robot with a maximum enclosed envelope of one cubic meter and maximum mass of 65 kg. The primary design objective is to maximize traversable distance over a range of outdoor terrain types while maintaining a high level of mobility. Here, mobility is quantified by the system kinematic isotropy, the ability of an ASOC module to maintain ground contact, the maximum traversable obstacle height, and the stability of the robot. The robot must operate under its own power, and therefore should maximize mass efficiency to increase its battery payload. It should also minimize power loss from motion resistance in deformable terrain. Factors influencing the design space include wheel width, wheel radius, ASOC split and offset lengths, and the number and relative location of ASOC modules. Geometric constraints that bound the allowable design space must also be considered.

Figure 14 shows an illustration of an omnidirectional mobile robot driven by four ASOC modules. This is a representative configuration that will be considered in this work; however the following analysis is general and applies to robots with N ASOC modules.
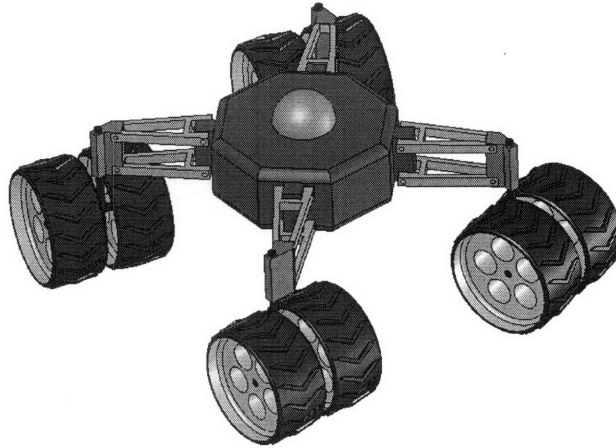
Figure 14. Illustration of an ASOC-driven omnidirectional mobile robot. This robot has four ASOC modules spaced at 90° intervals.

3.1 Geometric Constraints

The unique geometry of the ASOC and the large range of motion of each module constrain the size of some mechanical components. Potentially, a control algorithm could utilize the robot's redundancy to relax these constraints (by ensuring that wheel pairs are never directly oriented towards each other, for example). However, such an algorithm would likely reduce overall system mobility. Therefore, a geometric analysis of the ASOC module workspace is presented here.

3.1.1 ASOC Workspace Analysis

The maximum allowable wheel size that does not risk ASOC interference can be calculated by simple geometric analysis of the module workspace. As seen in Figure 15, the minimum distance between adjacent ASOC axes, d_a, must be at least twice the maximum radius of the ASOC module workspace, $r_{workspace}$. This radius is the distance from the vertical axis to the most distal point on the wheel:

$$r_{wheel.envelope} = \sqrt{\left(L_{offset} + r_{wheel}\right)^2 + \left(0.5L_{split} + t_{wheel}\right)^2} \; , \qquad (5)$$

where L_{offset} and L_{split} are the ASOC split and offset lengths, respectively, and r_{wheel} and t_{wheel} are the wheel radius and width, respectively.
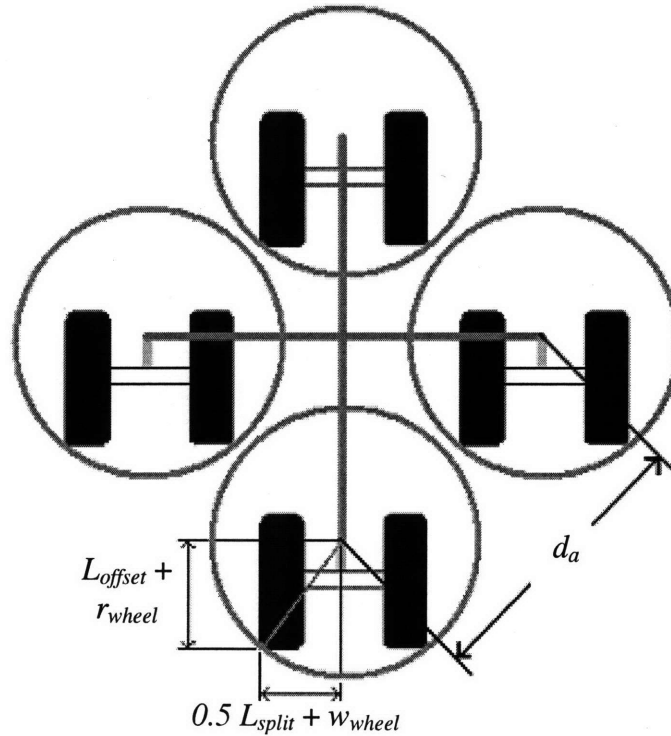

Figure 15. The circles represent the boundaries of the ASOC module workspace. To avoid ASOC interference, they should not intersect.

3.1.2 Maximum Pivot Angle Analysis

In rough terrain, the passive pivot axis (see Figure 6) allows the ASOC wheels to conform to terrain unevenness. A potential limiting factor of the pivot axis travel is wheel-shaft interference (see Figure 16).
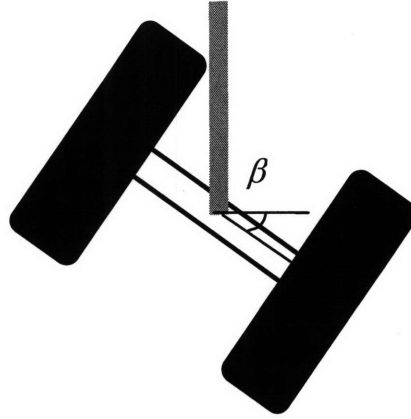
Figure 16. Rear view of an ASOC with near wheel-shaft interference.

The maximum allowable rotation angle of β can be calculated as the angle at which the inner rim of the wheel intersects with the vertical shaft that connects the module to the robot body. This occurs when

$$0.5L_{split} \cos \beta = r_{wheel.effective} \sin \beta \qquad (6)$$

where β is the angle of the pivot rotation and $r_{wheel.effective}$ is the vertical distance from the center of the wheel to the section of the rim that intersects the shaft, as shown in Figure 17. The value is calculated as

$$r_{wheel.effective} = \sqrt{r_{wheel}^2 - L_{offset}^2} \; . \qquad (7)$$

Figure 17. Depiction of $r_{wheel.effective}$.

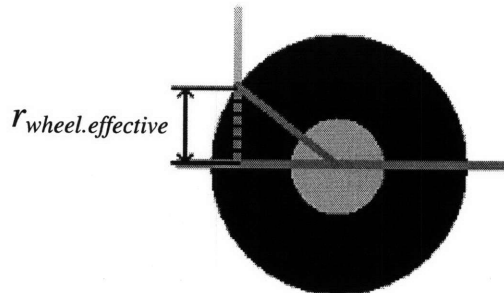Note that when $L_{offset} > r_{wheel}$, the shaft and wheel cannot interfere. However, such a configuration would potentially cause obstacles to collide with the ASOC axis before they contact the wheels, which is undesirable. In a nominal configuration, the maximum value of β is given as

$$\beta_{\max} = \tan^{-1}\left(\frac{0.5L_{split}}{\sqrt{r_{wheel}^2 - L_{offset}^2}}\right). \tag{8}$$

For reference, an ASOC with $L_{split} = 20$ cm, $L_{offset} = 10$ cm, and $r_{wheel} = 20$ cm would have a maximum allowable pivot angle of $30°$.

3.1.3 Maximum Suspension Travel Analysis

The suspension travel may be limited by wheel-suspension interference. The suspension elements should be designed to allow for maximum travel regardless of ASOC pose.

A desired maximum suspension travel can be derived from the desired maximum traversable step height. A rule of thumb in mobile robot design is to allow the suspension to bring the wheel high enough so that 2/3 of the wheel diameter is above the step. An active suspension component would assist in the climbing ability.
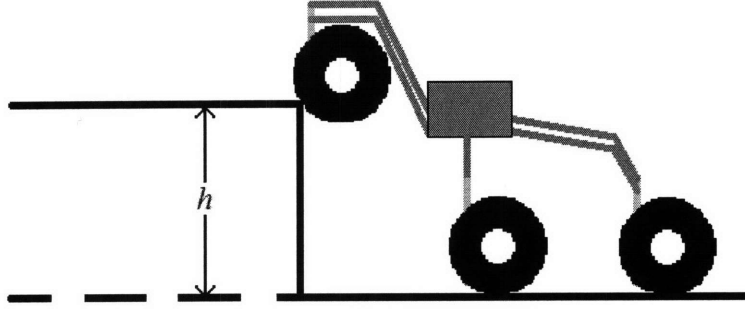
Figure 18. A robot utilizing its suspension capabilities to climb a high step. Note the near wheel-suspension interference for the left and the near suspension-suspension interference for all wheels.

3.2 Design Optimization

A full factorial design optimization was performed using the objectives discussed in Section III (system kinematic isotropy, the ability of an ASOC module to maintain ground contact, maximum traversable obstacle height, and robot stability) and constraints outlined in Section 3.1 (workspace limitations, module interference, and maximum suspension travel). The optimization parameters are the number of ASOC modules, L_{split}, L_{offset}, r_{wheel}, and w_{wheel}. An objective function, J, is expressed as a sum of the normalized mobility parameters:

$$J = \frac{K}{K^*} + \frac{\beta_{max}}{\beta_{max}^*} + \frac{h}{h^*} + \frac{d_{max}}{d_{max}^*} + \frac{S}{S^*} \,, \qquad (9)$$

where K is the kinematic isotropy, β_{max} is the maximum β axis pivot, h is the maximum obstacle height, d_{max} is the maximum traversable distance, and S is a measure of the robot's stability. The star superscript refers to the maximum value of each parameter in the design space. The optimization consisted of a full factorial analysis over the design

27

space to maximize the value of J.

In this analysis, kinematic isotropy and the maximum pivot angle and are calculated as described Sections 2.2 and 3.1.2, respectively. The maximum obstacle height is assumed to be a linear function of the wheel radius.

The optimization algorithm estimates maximum traversable distance by first determining the maximum available onboard energy. For the purposes of this study, it is assumed that the robot is powered by batteries with an energy density ρ_{energy} of 576 kJ/kg (similar to that of lithium-ion batteries [18]). The maximum allowable onboard battery mass, $M_{battery}$, is the difference between the non-battery mass (i.e., wheels, structural components, electronics, etc.) and the predetermined total allowable mass. In this study, the mission specific total available mass limit was 65 kg. The fixed mass (for structure and electronics) was 15% of the total allowable mass. Each ASOC (without wheels) weighed 5% of the total allowable mass. Wheel masses where computed assuming cylindrical geometry and the wheels radius and width, with a density equal to that of rubber (920 kg/m^3) [19].

The energy consumed during forward travel is then estimated using an expansion of a semi-empirical formulation for compaction resistance on deformable terrain [20].

$$CR = \frac{n_{wheels}}{\lambda^{\left(\frac{2n+2}{2n+1}\right)}(n+1)w_{wheel}^{\left(\frac{1}{2n+1}\right)}\left(k_c\Big/w_{wheel}+k_\phi\right)^{\left(\frac{1}{2n+1}\right)}}\left[\frac{\dfrac{Mg}{n_{wheels}}}{\sqrt{r_{wheel}}}\right]^{\left(\frac{2n+2}{2n+1}\right)},$$

$$\lambda = 1 - \frac{n}{3} + \frac{n(n-1)}{10} - \frac{n(n-1)(n-2)}{42} + \frac{n(n-1)(n-2)(n-3)}{216} \tag{10}$$

28

In (10), CR is the compaction resistance (N), M is the total robot mass (kg), n_{wheels} is the number of wheels (i.e., twice the number of ASOC modules), and n, k_c, and k_ϕ are terrain physical constants (shown in Table III [21, 22]). Note that this estimate holds for straight-line driving and does not consider other resistive forces (such as bulldozing forces) or energy used by other onboard devices.

TABLE III
TERRAIN PARAMETERS

Terrain type	n	k_c (kPa/m^{n-1})	k_ϕ (kPa/m^n)
Dry sand	1.1	0.9	1523.4
Sandy loam	0.7	5.3	1515.0
Clayey soil	0.5	13.2	692.2
Snow	1.6	4.4	196.7

The maximum traversable distance is approximated as

$$d_{max} = \frac{M_{battery}\rho_{energy}}{CR}.$$

(11)

Since the optimization compares similar systems, motor and drivetrain efficiencies are assumed identical for all candidate designs and therefore are not considered in the calculations.

The robot's tipover stability is also considered in the optimization. A stability measure (S) is calculated by taking the minimum distance from the center of the robot to the edges of the support polygon over the full joint space of the ASOC modules. Here, the vertices of the support polygon are defined by the points between each ASOC wheel pair, as shown in Figure 15. This is a conservative estimate, as defining the vertices by each ground contact point will result in a larger polygon.
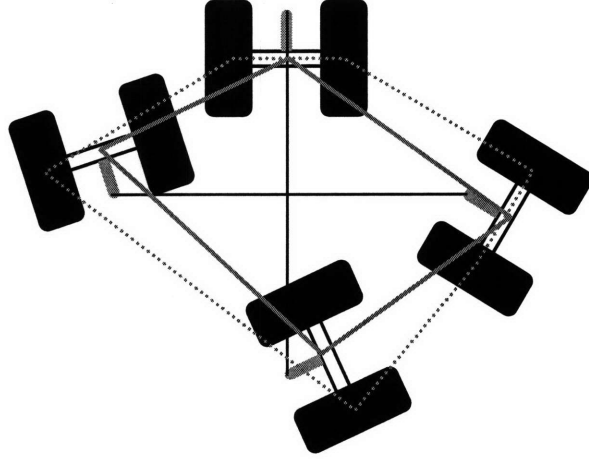
Figure 15. The solid gray polygon represents the estimated support polygon used in the optimization. It is bounded inside the true support polygon, shown as a dotted gray polygon.

3.3 Design Optimization Results

Table IV compares the values of the optimized mobility parameters of robots with three, four, and five ASOC modules. The robots were optimized for sandy loam. Results are presented relative to the robot with three ASOC modules. It can be observed that all four mobility parameters decrease as the number of ASOC modules increases.

TABLE IV
EFFECT OF NUMBER OF ASOCs ON MOBILITY PARAMETERS

# ASOCs	K	β_{max}	h	d_{max}	S
3	0%	0%	0%	0%	0%
4	-0.4%	-1.3%	-6.1%	-38.8%	94.9%
5	-2.2%	16.2%	-60.9%	-52.9%	161.4%

A robot with four ASOC modules has similar values of kinematic isotropy (K), maximum β axis pivot angle (β_{max}), and maximum traversable obstacle height (h) as a three ASOC robot, however, adding the fourth module decreases available battery mass, and therefore decreases d_{max}, but increases the size of the support polygon, and therefore increases the stability measure (S). A fifth ASOC module requires smaller wheels,

30

resulting in lower maximum traversable obstacle height, but higher maximum β axis pivot angle.

Table V shows the values of the optimized geometric parameters for a three ASOC robot. Optimized values were calculated for each of the four terrain types shown in Table III, assuming rough terrain with an angle range of 0-30°. All terrain angles within the range were given equal likelihood. Table VI shows the change in mobility parameter values for optimized designs compared to a baseline design with parameters determined by engineering judgment (L_{offset} = 0.15 m, L_{split} = 0.20 m, r_{wheel} = 0.15 m, w_{wheel} = 0.03 m).

TABLE V
GEOMETRIC PARAMETERS FROM OPTIMIZATION

Terrain type	L_{offset} (m)	L_{split} (m)	r_{wheel} (m)	w_{wheel} (m)
Dry sand	.144	.325	.148	.090
Sandy loam	.134	.306	.139	.126
Clayey soil	.134	.306	.139	.133
Snow	.144	.325	.148	.054

TABLE VI
MOBILITY PARAMETER INCREASES FROM OPTIMIZATION

Terrain type	K	β_{max}	H	d_{max}	S
Dry sand	13.2%	85.2%	-1.4%	18.1%	1.4%
Sandy loam	12.8%	82.8%	-7.4%	35.2%	3.6%
Clayey soil	12.8%	82.8%	-7.4%	31.9%	3.6%
Snow	13.2%	85.2%	-1.4%	3.3%	1.4%

In all cases, the optimized offset lengths were slightly smaller than the wheel radii, which yielded large allowable β tilt angles. The L_{split} / L_{offset} values were all near 2.27:1, thus maximizing isotropy for the given terrain roughness range.

As presented, the optimized parameter values for the relatively deformable

31

terrains (i.e. dry sand and snow) resulted in wheels with larger radii but narrower widths compared to those optimized for relatively rigid terrains (i.e. sandy loam and clayey soil). The thinner widths lead to decreased wheel weight. One could also minimize ground pressure by choosing a wider wheel with smaller radius, but for a given a depth of sinkage, a tall, narrow wheel has significantly less compaction resistance than a short, wide one. For the relatively rigid terrains, a wider wheel was preferred as it allowed a greater amount of onboard battery mass, thus increasing maximum traversable distance.

3.4 Suspension Design Considerations

In this section, a potential suspension design is presented. This suspension system could be hybrid active and passive which would allow the passive element to provide quick response to terrain roughness while the active portion could assist in step climbing or reconfiguration for different parts of a mission. It is also designed to allow for the maximum range of motion for all components.

The basic construction of the suspension design presented here is a 4-bar linkage. This configuration allows for a large vertical displacement with a relatively small horizontal module displacement, thus keeping all modules a similar distance from the robot center which increases isotropy. This also keeps the vertical ASOC axes parallel to the robot body's vertical axis, simplifying control and keeping the effective L_{offset} constant. The spring/damping/actuation elements could be connected between the lower arm and the body.

If a conventional four bar linkage suspension is utilized on this robot, upward displacement is limited by interference between the wheels and suspension arms (see

Figure 19(a)). The arms could be shaped to avoid wheel-arm interference, as shown in Figure 19(b).

As shown in Figure 20(a,b), the downward displacement is significantly lower using the shaped four bar linkage. Splitting the top bar into two halves (Figure 21), eliminates interference between the top and bottom bars, greatly increasing both upward (Figure 19(c)) and downward displacement (Figure 20(c)).

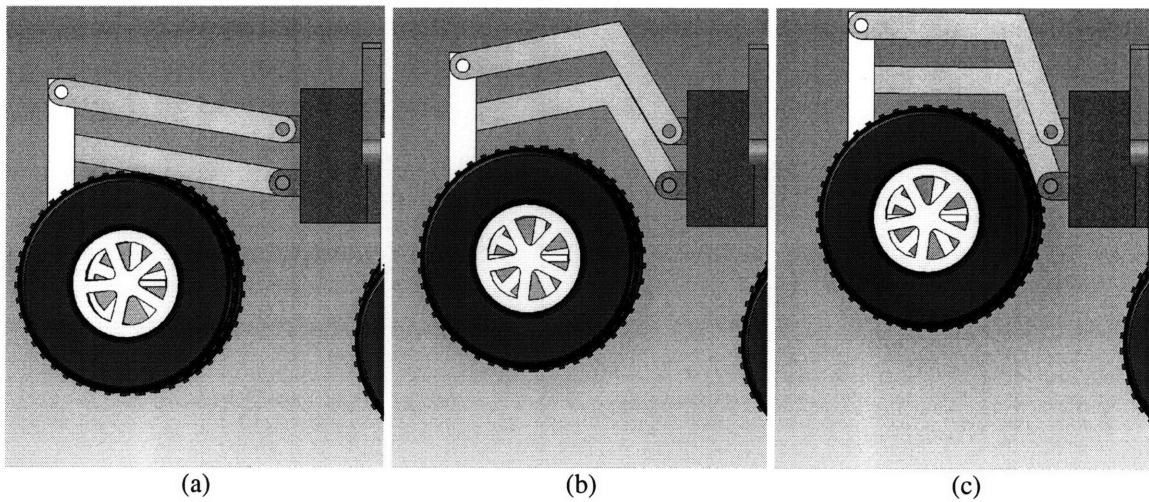(a)   (b)   (c)

Figure 19. Maximum upward suspension displacement for a straight four bar linkage (a), shaped four bar linkage (b), and shaped-split four bar linkage (c).

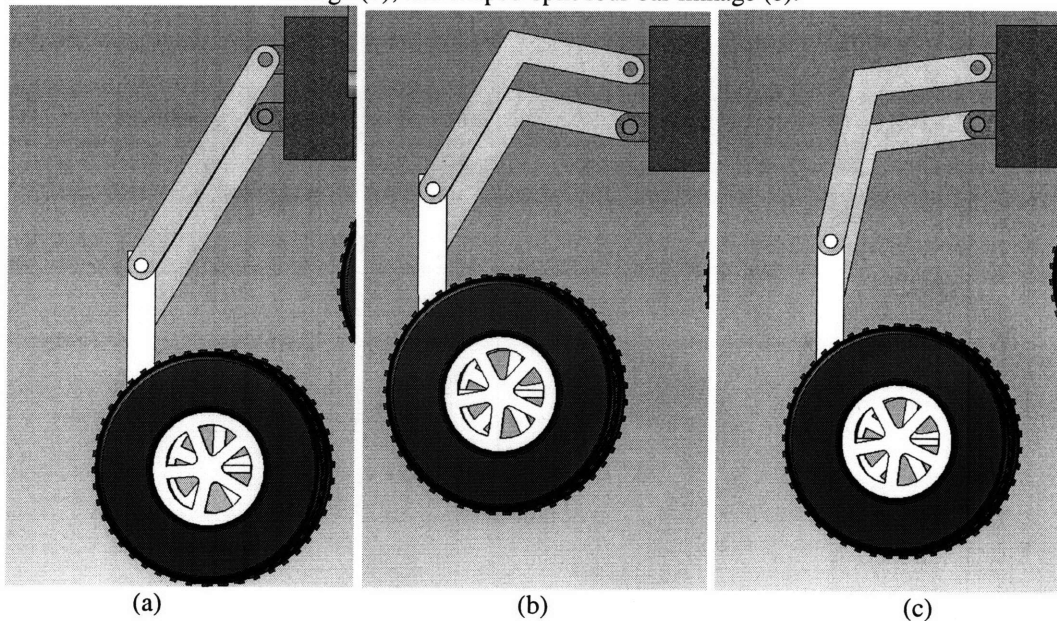(a)   (b)   (c)

Figure 20. Maximum downward suspension displacement for a straight four bar linkage (a), shaped four bar linkage (b), and shaped-split four bar linkage (c).
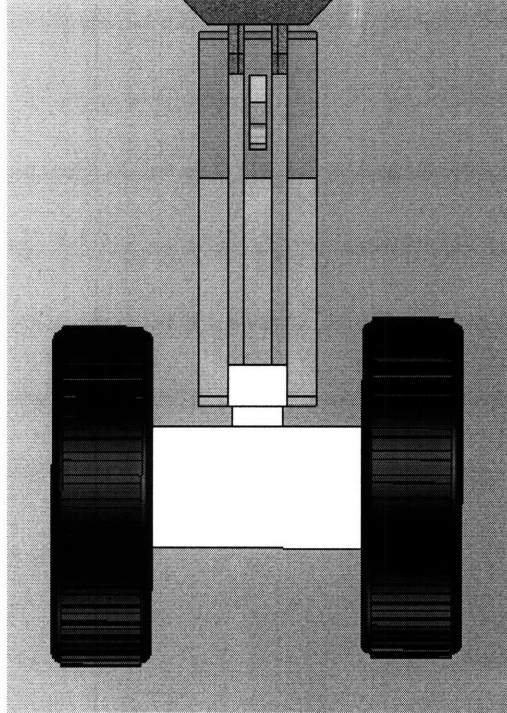
Figure 21. Top view of the shaped-split four bar linkage. The center bar corresponds to the bottom bar of the four bar linkage in Figure 20(c). The left and right bars are the split halves of the top bar in Figure 20(c).

3.5 Point Robot Design

This section illustrates a point robot design with four ASOC modules (Figure 22). This robot utilizes the shaped-split four bar linkage described in Section 3.4 to achieve a maximum suspension travel of 0.33 m. The wheels have a 0.163 m radius, the largest allowed given a body length (L_{body}) of 1 m and the workspace constraints outlined in Section 3.1.1 (see Figure 23). A maximum pivot angle of 30° and a high isotropy is achieved by have an L_{split} of 0.21 m and an L_{offset} of 0.10 m (see Sections 3.1.2 and 2.5) yielding L_{split} / L_{offset} = 2.1.
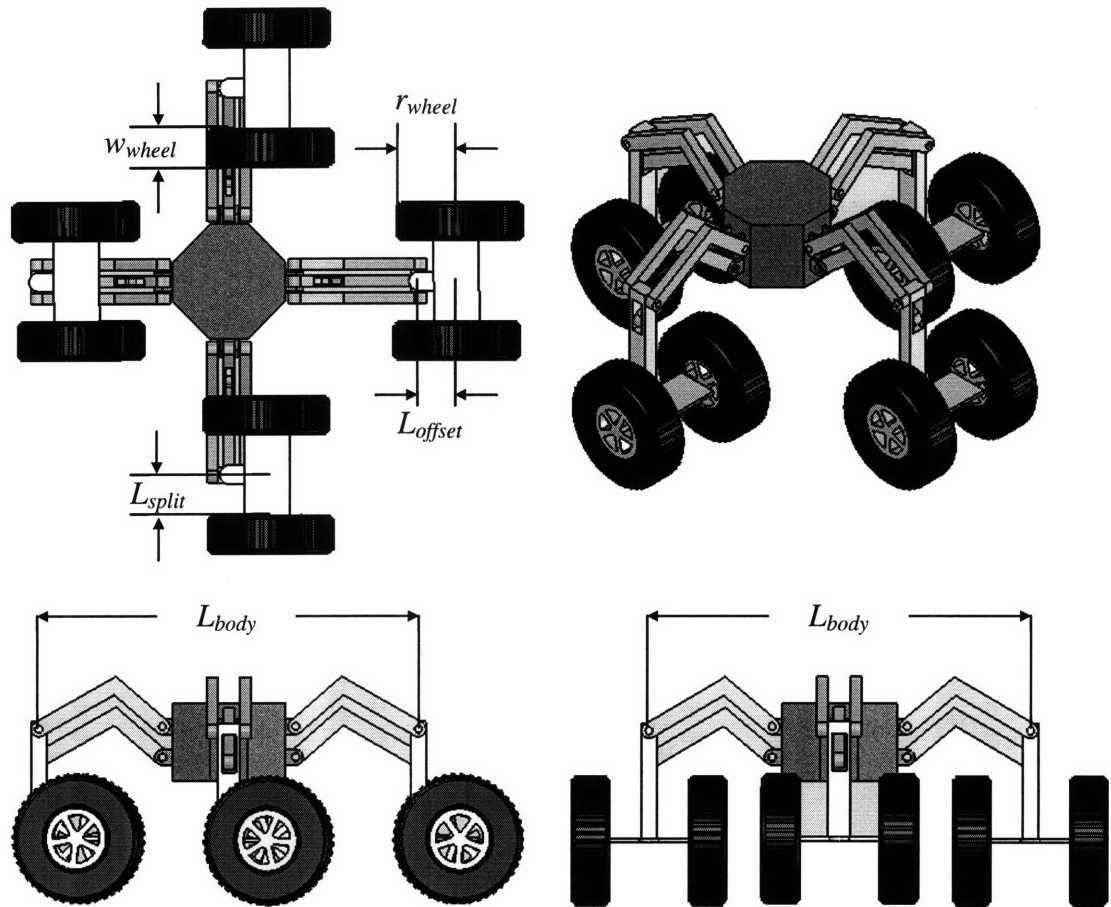
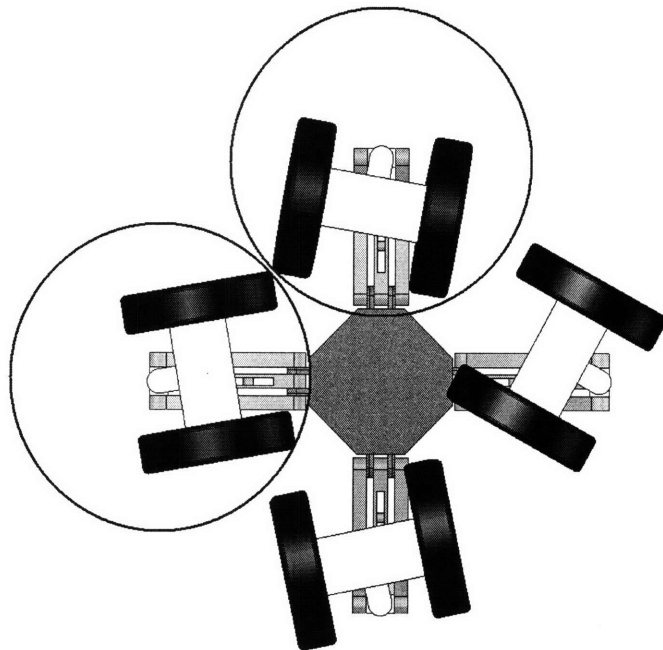Figure 22. A four view drawing of a point robot design.

Figure 23. Bottom view of a point robot design. Note that the ASOC modules are the maximum size allowed without violating workspace constraints outlined in Section 3.1.1.

IV. KINEMATIC ANALYSIS AND CONTROL

The previous section presented analysis of an ASOC driven omnidirectional mobile robot for operation in rough terrain. During operation, control systems must coordinate ASOC motion while adapting to terrain unevenness. This section presents a kinematic controller that allows omnidirectional mobility in rough terrain.

4.1 Kinematic Analysis

The kinematics of an omnidirectional mobile robot model were analyzed. The coordinate frames were defined using Devanit-Hartenberg (D-H) notations shown in Table VIII. Coordinate frame assignments are shown in Figure 24.

TABLE VIII
JOINT REPRESENTATION IN D-H NOTATION

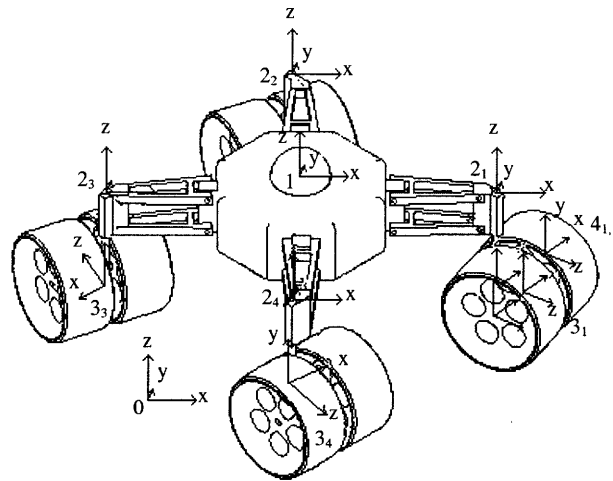| Joint number	d_i	ζ_i	a_i	ξ_i
1_n	0	$2\pi(n-1)/N$	r	0
2_n	h	$-(\alpha + \pi/2)$	0	$\pi/2$
3_n	L_{offset}	$-\beta$	0	0
$4_{n,m}$	0	0	$\pm L_{split}/2$	0

Figure 24. Coordinate frame assignments for an ASOC-driven omnidirectional mobile robot. Note that some wheel and axle frames are hidden for clarity.

In the notation above, d_i is the distance between frame i and frame $i+1$ along the z_{i+1} axis, ζ_i is the angle between x_i and x_{i+1} about z_{i+1}, a_i is the distance from z_i to z_{i+1} along x_{i+1}, ξ_i is the twist angle between z_i and z_{i+1} about x_{i+1}, n is the ASOC number, m is the wheel number, r is the body radius, and h is the vertical distance from the ASOC base to the robot body.

Here a three-dimensional model is considered. A body-fixed frame ("1") is allowed 6 DOF with respect to an inertial frame ("0"). The interface of each ASOC module link and the robot body/suspension frame ("2_n" where n refers to the ASOC number and N is the total number of ASOCs) is defined on the body a distance r from the center of the body. A frame ("3_n") at the bottom of each ASOC module link is a distance h below the previous frame and can rotate about axis α. The next frame ("4_n") is defined on the axle at the midpoint between the wheels, and can rotate about β. For convenience, a frame is also defined at the center of each wheel ("$5_{n,m}$") where n refers to the ASOC number and m refers to the wheel number). These redundant frames are fixed with respect to the axle frame. There is no specified wheel-ground contact frame, as each wheel may have no contact or several moving contact points.

Coordinate transformation matrices are defined as follows:

$$T_1^{2_n} = \begin{bmatrix} \cos(2\pi(n-1)/N) & -\sin(2\pi(n-1)/N) & 0 & r \\ \sin(2\pi(n-1)/N) & \cos(2\pi(n-1)/N) & 0 & 0 \\ 0 & 0 & 1 & 0 \\ 0 & 0 & 0 & 1 \end{bmatrix} \tag{12}$$

$$T_{2_n}^{3_n} = \begin{bmatrix} \cos(-(\alpha_n + \pi/2)) & 0 & \sin(-(\alpha_n + \pi/2)) & 0 \\ \sin(-(\alpha_n + \pi/2)) & 0 & -\cos(-(\alpha_n + \pi/2)) & 0 \\ 0 & 1 & 0 & h \\ 0 & 0 & 0 & 1 \end{bmatrix} \qquad (13)$$

$$T_{3_n}^{4_n} = \begin{bmatrix} \cos(-\beta_n) & -\sin(-\beta_n) & 0 & 0 \\ \sin(-\beta_n) & \cos(-\beta_n) & 0 & 0 \\ 0 & 0 & 1 & L_{offset} \\ 0 & 0 & 0 & 1 \end{bmatrix} \qquad (14)$$

$$T_{4_n}^{5_{n,m}} = \begin{bmatrix} 1 & 0 & 0 & (-1)^m \dfrac{L_{split}}{2} \\ 0 & 1 & 0 & 0 \\ 0 & 0 & 1 & 0 \\ 0 & 0 & 0 & 1 \end{bmatrix} \qquad (15)$$

where $T_p{}^q$ is the matrix transforming motion from frame p into frame q. Thus the transformation from the body center frame to the wheel n,m frame is

$$T_1{}^{5_{n,m}} = T_1{}^{2_n} T_{2_n}^{3_n} T_{3_n}^{4_n} T_{4_n}^{5_{n,m}} \qquad (16)$$

Using these relations, the wheel velocities required to generate a desired body center velocity can be determined.

4.2 Kinematic Control

A simple kinematic control scheme has been developed based on the preceding

38

kinematic analysis. Given a desired body translational and rotational velocity defined in an inertial frame, the velocity for each ASOC wheel can be determined despite the effects of terrain unevenness.

First, the velocity of the link between the ASOC module and robot body is computed by:

$$\dot{\mathbf{x}}_{link} = \dot{\mathbf{x}}_{body} + \dot{\phi}r\begin{bmatrix} \cos(\varsigma_i) \\ \sin(\varsigma_i) \end{bmatrix} \tag{17}$$

where $\dot{\mathbf{x}}_{link}$ and $\dot{\mathbf{x}}_{body}$ are the planar velocity vectors of the link and body, respectively, $\dot{\phi}$ is the yaw rate of the body, and r and ς_i locate the link i in the body frame. Note that this control method aligns the thrust vectors of each ASOC with the direction of travel, minimizing loss producing internal forces. The wheel velocities that yield the desired ASOC link velocity are found as [17]:

$$\dot{\mathbf{x}}_{link} = \begin{bmatrix} \dfrac{1}{2}\cos(\alpha_n) - \dfrac{L_{offset}}{L_{split}}\sin(\alpha_n) & \dfrac{1}{2}\cos(\alpha_n) + \dfrac{L_{offset}}{L_{split}}\sin(\alpha_n) \\ \dfrac{1}{2}\sin(\alpha_n) + \dfrac{L_{offset}}{L_{split}}\cos(\alpha_n) & \dfrac{1}{2}\sin(\alpha_n) - \dfrac{L_{offset}}{L_{split}}\cos(\alpha_n) \end{bmatrix} \begin{bmatrix} V_{n,1} \\ V_{n,2} \end{bmatrix} \tag{18}$$

and hence:

$$\begin{bmatrix} V_{n,1} \\ V_{n,2} \end{bmatrix} = \begin{bmatrix} \dfrac{1}{2}\cos(\alpha_n) - \dfrac{L_{offset}}{L_{split}}\sin(\alpha_n) & \dfrac{1}{2}\cos(\alpha_n) + \dfrac{L_{offset}}{L_{split}}\sin(\alpha_n) \\ \dfrac{1}{2}\sin(\alpha_n) + \dfrac{L_{offset}}{L_{split}}\cos(\alpha_n) & \dfrac{1}{2}\sin(\alpha_n) - \dfrac{L_{offset}}{L_{split}}\cos(\alpha_n) \end{bmatrix}^{-1} \dot{\mathbf{x}}_{link} \qquad (19)$$

where $V_{n,m}$ is the forward linear velocity of a wheel n,m in the wheel frame ("$5_{n,m}$"), and is computed as $V_{n,m}=R\omega_{n,m}$ where R is the wheel radius and $\omega_{n,m}$ is the wheel angular speed. Angular velocity is controllable via simple PD or other schemes.

Terrain roughness causes ASOC modules to tilt (i.e. rotate about β) and the wheel velocities to have components out of the body's x-y plane. The controller must compensate for module tilt via computation of an effective L_{split}, (see Figure 12). The projection of wheel velocity onto the body's x-y plane is used on the left side of (20). Including the tilt compensation and out plane wheel velocity computation in (19) yields:

$$\begin{bmatrix} V_{n,1}\cos\gamma_{n,1} \\ V_{n,2}\cos\gamma_{n,2} \end{bmatrix} = \begin{bmatrix} \dfrac{1}{2}\cos(\alpha_i) - \dfrac{L_{offset}}{L_{split}\cos(\beta_i)}\sin(\alpha_i) & \dfrac{1}{2}\cos(\alpha_i) + \dfrac{L_{offset}}{L_{split}\cos(\beta_i)}\sin(\alpha_i) \\ \dfrac{1}{2}\sin(\alpha_i) + \dfrac{L_{offset}}{L_{split}\cos(\beta_i)}\cos(\alpha_i) & \dfrac{1}{2}\sin(\alpha_i) - \dfrac{L_{offset}}{L_{split}\cos(\beta_i)}\cos(\alpha_i) \end{bmatrix}^{-1} \dot{\mathbf{x}}_{link} \qquad (20)$$

where $\gamma_{n,m}$ is the angle between the velocity vector of wheel n,m and the x-y plane in the body-fixed frame (see Figure 25).
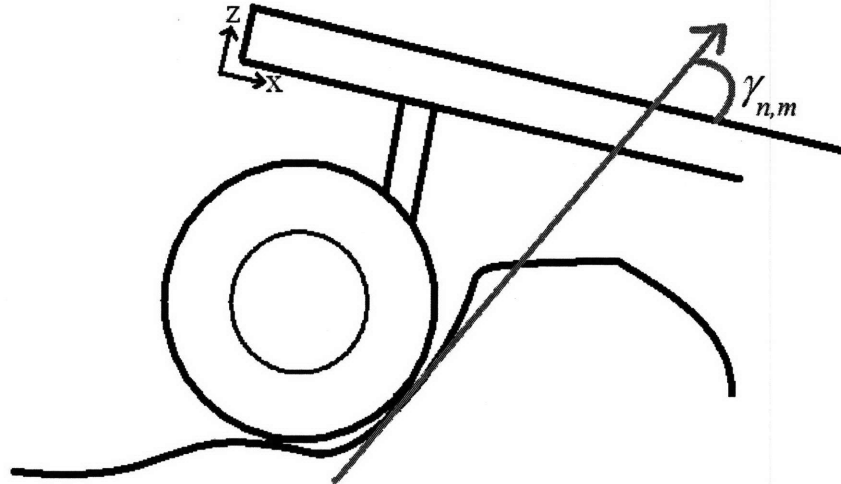
Figure 25. Wheel inclination angle, $\gamma_{n,m}$. The gray vector is parallel to the velocity of the wheel.

Figure 26 shows a block diagram of a scheme for rough terrain omnidirectional mobile robot control. The input is a desired velocity profile defined in the inertial frame. It is assumed that the robot's full state can be estimated. The desired velocity profile is converted to a desired velocity in the body-fixed frame based on the robot's current position and orientation. ASOC module link velocities are then computed via (17). Desired wheel velocities can then be calculated using (20), here assuming knowledge or estimates of local terrain inclination. Terrain inclination can be estimated via axle-mounted force sensors (to measure wheel-terrain interaction normal force direction) or via kinematic estimators [21]. PD controllers command each wheel to track the desired wheel velocities. Actual velocities can be determined via odometry; however more sophisticated methods are required to estimate wheel slip [24-26].
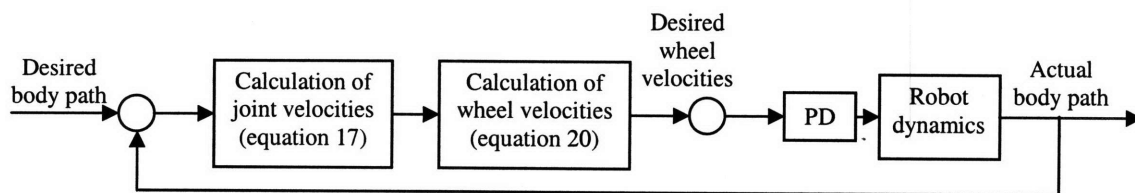

Figure 26. Control scheme of an omnidirectional mobile robot.

41

4.3 Simulation Results

A dynamic model of an ASOC-driven mobile robot was developed to study the performance of the control method described above. The kinematic controller described in (17) and (20) was implemented to allow the robot to track a desired velocity profile over flat and rough terrain. Independent PD control loops allowed each wheel to track its desired velocity.

The robot parameters for the simulation were as follows: body length=1 m, total mass=65 kg, wheel radius=0.10 m, L_{split}=0.20 m, L_{offset}=0.10 m. The control gains for each wheel were K_p=7.3, K_d=0.02. Wheel-terrain interaction forces were determined via a simple coulomb friction model with μ=0.6. Terrain elevation was modeled as a triangularized mesh with elevation points possessing a standard deviation of σ. In initial simulations it was assumed that the robot possessed perfect knowledge of terrain inclination. Wheel-terrain contact locations were determined by making a thin wheel approximation and finding the intersection points between the wheel and the local triangular mesh patches.

To study the omnidirectional capability of the robot, a desired 4.5 m square path was commanded at a constant speed of 1.5 m/s. This corresponds to 1.5 body lengths/second.
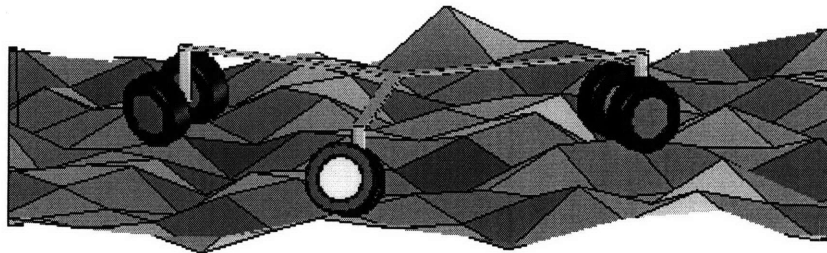

Figure 27. View of a terrain section to demonstrate the scale of the robot with $\sigma = 4.5$.
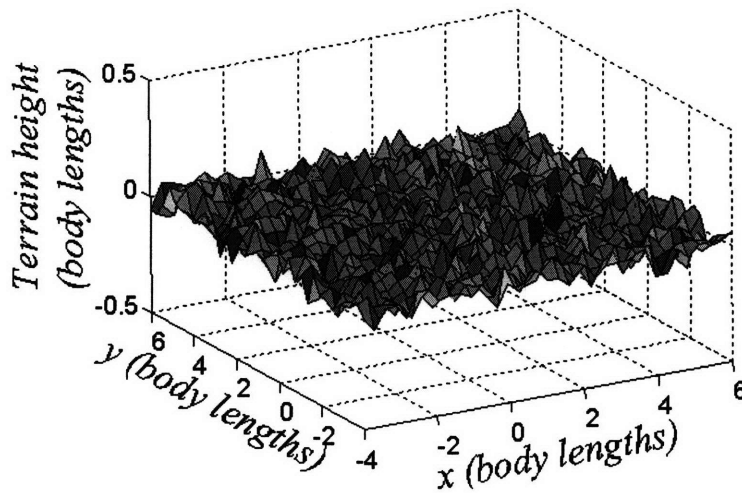
Figure 28. Example of terrain used in simulation, with σ = 4.5.

In the following simulations, σ was chosen as 0, 1.5, 3.0, and 4.5 cm, yielding

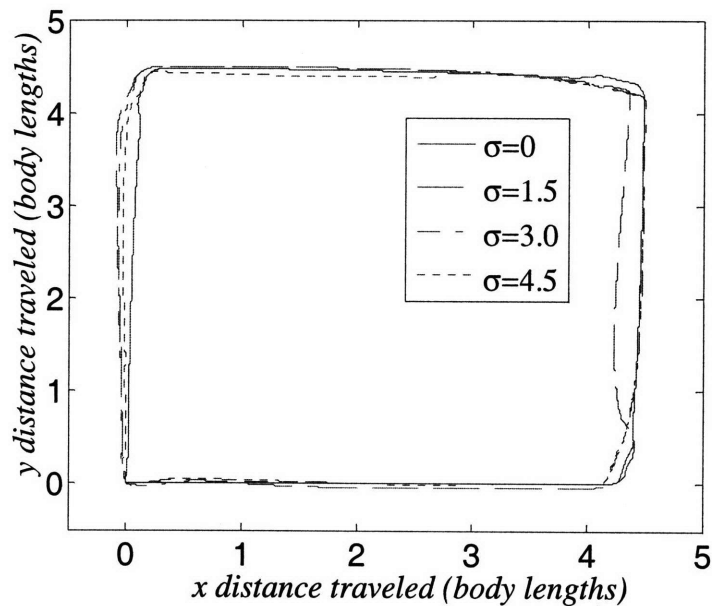maximum terrain inclination angles of approximately 0°, 20°, 35°, and 45°, respectively.

Figure 29. Top view of robot path during square tracking on rough terrain.

In Figure 29 it can be seen that the robot was able to track the desired path with

relatively good fidelity, even in very rough terrain. In these simulations, the controller

had accurate, continuous absolute position data. Table IX presents the RMS error for this trial for each terrain roughness.

σ	RMS error (% body)
0.0	8.67
1.5	8.89
3.0	10.48
4.5	11.59

Although an omnidirectional robot can kinematically perform zero radius turns at any velocity, dynamic effects may reduce path tracking at higher velocities. Figure 30 shows that the robot is able to maintain a high velocity magnitude when the body was changing direction. During these simulations, the velocity magnitude never dropped below 48% of the nominal commanded level.
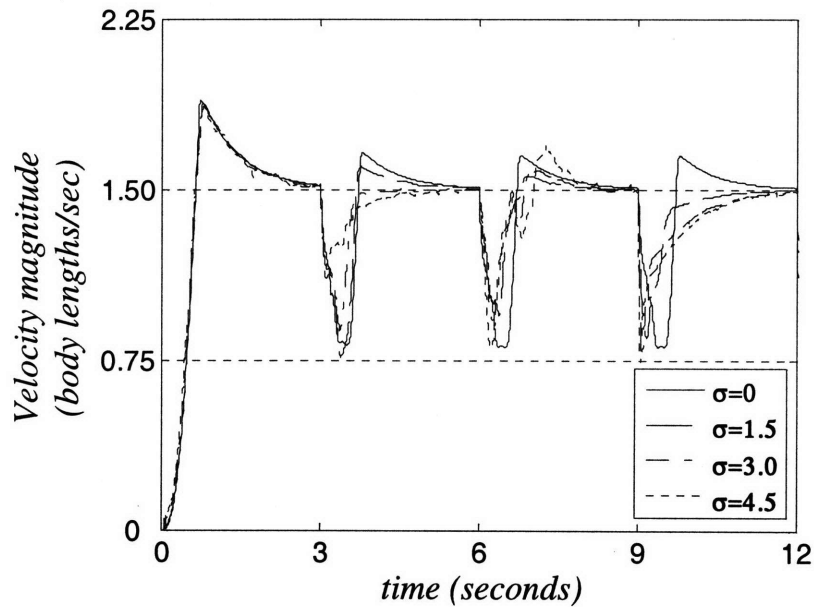

Figure 30. Velocity magnitude during path tracking.

44

Further simulations were conducted to study the effects of utilizing local terrain inclination knowledge in the controller and knowledge of robot absolute position in the inertial frame. Simulations were run with and without absolute position updates at 0.5 Hz and with and without terrain knowledge. Simple dead reckoning was used estimate robot position in simulations without absolute position knowledge and to interpolate between updates in simulations with absolute position knowledge. Path tracking results are shown in Figure 31. Numerical results are shown in Table X.

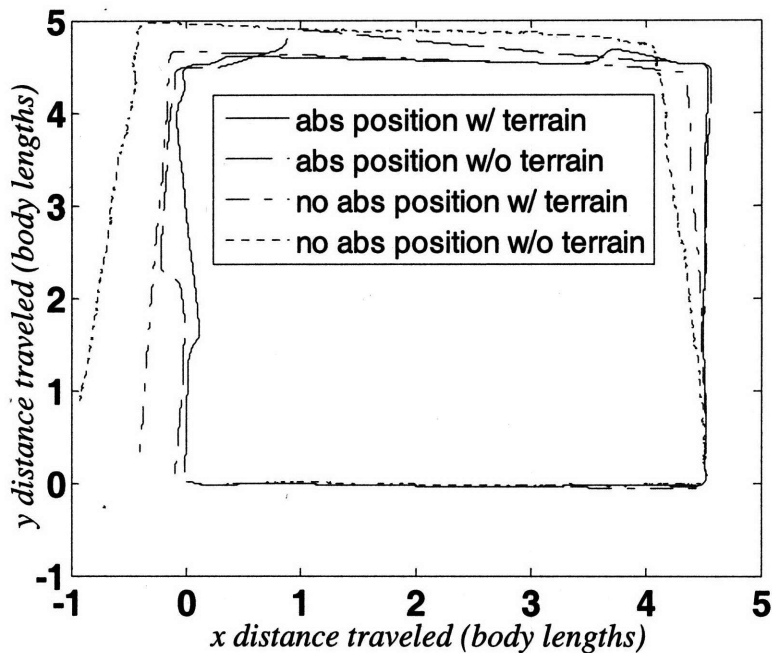Figure 31. Top view of the body trace during square tracking on rough terrain for varying levels of controller knowledge.

TABLE X
RMS PATH TRACKING ERROR FOR VARYING CONTROLLER KNOWLEDGE

Controller Knowledge	RMS error (% body)
Absolute position w/ terrain	6.96
Absolute position w/o terrain	17.71
No absolute position w/ terrain	21.28
No absolute position w/o terrain	86.31

45

Note that the path tracking error in simulations with absolute position information is bounded, while the tracking error in simulations without absolute position data is not. When absolute position information is not available, a 75.3% reduction in path tracking error is seen when the robot controller uses local terrain inclination information (both errors are unbounded). This is useful for the many situations where position information from GPS, for example, may be unavailable. Even with absolute position updates, path tracking error is reduced by 60.7% when the controller uses local terrain inclination information (both errors are bounded).

V.   SUMMARY AND FUTURE WORK

In this thesis, the effectiveness of an omnidirectional mobile robot driven by active split offset casters for use in rough terrain has been studied. An isotropy analysis was conducted to determine the optimal geometry and layout of the ASOC modules. This analysis indicates that equally spaced modules with L_{split} / L_{offset} = 2.0 yield a robot with equal mobility capability in all directions on flat terrain. On rough terrain, a larger ratio is desired, and robot isotropy degrades slightly. It also shows that isotropy is independent of wheel radius, which increases the scalability of the design.

Numerous design considerations for omnidirectional mobile robots were presented. An optimization algorithm was implemented to derive values for ASOC module and wheel geometries. For illustration, a man portable robot was designed, but the geometric constraints and the optimization algorithm are scalable and can be applied to robots of any size. It was shown that the designs suggested by the optimization have improved performance when compared to a non-optimized design. Through deliberate ASOC geometric parameter selection, it was possible to increase estimated traversable distance and mobility versus a baseline design.

A kinematic controller was developed and its performance was studied on both flat and rough terrain. The effects of local terrain inclination information and absolute position knowledge on performance were studied. Simulation results showed that an omnidirectional mobile robot is able to track a square trajectory with good performance despite local terrain inclinations angles near 45°. It was also shown that substantial path tracking improvements were possible if local terrain inclination information was used in the controller.

47

This work presented many design guidelines for an omnidirectional mobile robot. To continue this aspect of the work, further considerations, such as hardware selection and component placement must be performed. As the robot is intended for rough terrain, suspension design is crucial. A sensor suite should also be selected for the intended robot application. When the remaining design decisions are completed, the robot must be assembled and tested, with deviations from simulated performance considered.

To quantitatively determine the advantage of an omnidirectional mobile robot over a traditionally steered robot, a universal mobility metric should be developed. While the isotropy metric is useful for comparing various omnidirectional mobile robot designs, its value is simply 0.0 for anything else. Some sacrifices must be made to allow a mobile robot to move omnidirectionally. For example, while an ASOC driven mobile robot has a distinct advantage in cornering, the design constraints require it to use smaller wheels than would be permissible on an Ackermann steered robot of the same size. A universal mobility metric would assist in determining when these trade-offs are desirable.

REFERENCES

[1]   Fish, S., "UGV's in Future Combat Systems," *Proceedings of SPIE - The International Society for Optical Engineering*, v 5422, *Unmanned Ground Vehicle Technology VI*, pp. 288-291, Apr 2004.

[2]   Blitch, J., "Artificial Intelligence Technologies for Robot Assisted Urban Search and Rescue," *Expert Systems with Applications*, 1996.

[3]   Erickson, J., "Living the Dream: An Overview of the Mars Exploration Project," *IEEE Robotics and Automation Magazine*, v 13, n 2, pp. 12-18, Jun 2006.

[4]   Cheng, J., Gao, L., Wang, H., "Steering Analysis of Tracked Vehicles Based on Skid Condition," *Chinese Journal of Mechanical Engineering*, v 42, pp. 192-195, May 2006.

[5]   Ishigami, G., Miwa, A., Yoshida, K., "Steering Trajectory Analysis of Planetary Exploration Rovers Based on All-Wheel Dynamics Model," *Proceedings of the 8th International Symposium on Artificial Intelligence, Robotics and Automation in Space*, pp. 121-128, 2005.

[6]   Iagnemma, K. and Dubowsky, S., *Mobile Robots in Rough Terrain: Estimation, Motion Planning, and Control with Application to Planetary Rovers*, Springer Tracts in Advanced Robotics (STAR) Series, Vol. 12, Springer, 2004.

[7]   Fujisawa, S., Ohkubo, K., Yoshida, T., Satonaka, N., Shidama, Y., and Yamaura, H., "Improved Moving Properties of an Omnidirectional Vehicle Using Stepping Motor", *Proceedings of the 36th Conference on Decision & Control*. San Diego, California, pp.3654-3657, 1997.

[8]   Williams, R., Carter, B., Gallina, P., and Rosati, G., "Wheeled Omni-directional Robot Dynamics Including Slip," *Proceedings of 2002 ASME Design Engineering Technical Conferences,* Sep 2002.

[9]   Muir, P., and Neuman, C., "Kinematic Modeling for Feedback Control of an Omnidirectional Wheeled Mobile Robot," *Proc. of 1987 IEEE International Conference on Robotics and Automation,* 1987.

[10]   Bradley A., Miller, S., Creary, G., Miller, N., Begley, M., Misch, N., "Mobius, an Omnidirectional Robot Utilizing Mecanum Wheels and Fuzzy Logic Control," *Proceedings of the 28th Annual AAS Rocky Mountain Guidance and Control Conferences,* pp. 251-266, 2005.

[11]   Ferriere L., Raucent B., "ROLLMOBS, a New Universal Wheel Concept," *Proceedings of 1998 IEEE International Conference on Robotics and Automation,* pp. 1877-1882, Leuven, May 1998.

[12]   West, A.M., and Asada, H., "Design of Ball Wheel Mechanisms for Omnidirectional Vehicles with Full Mobility and Invariant Kinematics," *ASME Journal of Mechanical Design,* 117, 1995.

[13]   Carlson, J., Murphy, R., "How UGVs Physically Fail in the Field," *IEEE Transactions on Robotics,* v 21, n 3, Jun 2005.

[14]   Wood, C., Davidson, M., Rich, S., Keller, J., and Maxfield, R., "T2 Omni-Directional Vehicle Mechanical Design," *Proceedings of the SPIE Conference on Mobile Robots XIV,* Boston, pp. 69-76, Sep 1999.

[15]   Park, T., Lee, J., Yi, B., Kim, W., You, B., Oh., "Optimal Design and Actuator Sizing of Redundantly Actuated Omni-directional Mobile Robots," *IEEE*

International Conference on Robotics and Automation, pp.732-737, 2002.

[16]   Yu, H., Dubowsky, S., and Skwersky, A., "Omni-directional Mobility Using Active Split Offset Castors." *Proceedings of the 26th Biennial Mechanisms and Robotics Conference of the 2000 ASME Design Engineering Technical Conferences*, Sep 2000.

[17]   Spenko, M., Yu, H., and Dubowsky, S., "Analysis and Design of an Omnidirectional Platform for Operation on Non-Ideal Floors," *Proceedings of the 2002 IEEE International Conference on Robotics and Automation*, Washington, DC, May 2002.

[18]   Megahed, S., and Scrosati, B., "Lithium-Ion Rechargeable Batteries," *Journal of Power Sources*, V 51, Num. 1-2, pp 79-104, Aug-Sep 1994.

[19]   Treloar, LGR. *The Physics of Rubber Elasticity*. Oxford: Oxford University Press, 2005.

[20]   Bekker G. *Theory of land locomotion, the mechanics of vehicle mobility*. Ann Arbor: The University of Michigan Press; 1956.

[21]   Yong R, Fattah E, Skiadas N. *Vehicle traction mechanics*. Amsterdam: Elsevier Science Publishers; 1984.

[22]   Wong J. *Terramechanics and Offroad Vehicles*. Amsterdam: Elsevier Science Publishers; 1989.

[23]   Iagnemma, K. , Rzepniewski, A., Dubowsky, S., and Schenker, P., "Control of Robotic Vehicles with Actively Articulated Suspensions in Rough Terrain," *Autonomous Robots,* V 14, Num. 1, Jan 2003.

[24]   Reina, G., Ojeda, L., Milella, A., and Borenstein, J., "Wheel Slippage Detection

for Planetary Rovers," *IEEE/ASME Transactions on Mechatronics*, V 11, Num. 2, pp 185-195, April 2006.

[25] Volpe, R., Estlin, T., Laubach, S., Olson, C., and Balaram, J. , "Enhanced Mars Rover Navigation Techniques," *IEEE International Conference on Robotics and Automation,* pp.926-931, 2000.

[26] Nistér, D., Naroditsky, O., and Bergen, J., "Visual Odometry for Ground Vehicle Applications," *Journal of Field Robotics*, V 23, Num. 1, pp 3-20, Jan 2006.